IEEE Access
Multidisciplinary ⋮ Rapid Review ⋮ Open Access Journal

Received 26 February 2024, accepted 11 March 2024, date of publication 18 March 2024, date of current version 22 March 2024.

Digital Object Identifier 10.1109/ACCESS.2024.3377901

RESEARCH ARTICLE

Theory and Design of Doherty Power Amplifier With Active Harmonic Injection

Y. MARY ASHA LATHA, (Member, IEEE), LUÍS C. NUNES, (Senior Member, IEEE), FILIPE M. BARRADAS, (Member, IEEE), AND JOSÉ C. PEDRO, (Fellow, IEEE)

Instituto de Telecomunicações, Universidade de Aveiro, Campus Universitário de Santiago, 3810-193 Aveiro, Portugal

Corresponding author: Y. Mary Asha Latha (ymashalatha@ieee.org)

This work was supported in part by the Foundation for Science and Technology (FCT) and Portuguese Ministry of Science, Technology, and Higher Education (MCTES) through the National Funds and European Union (EU) Funds under Project UIDB/50008/2020-UIDP/50008/2020.

ABSTRACT This paper analyzes the performance of the Doherty power amplifier (DPA) with the injection of the second harmonic component generated by the carrier power amplifier (PA) into the peaking PA and vice-versa, using a harmonic injection network (HIN). A mathematical analysis is presented to estimate the second harmonic loads seen by the carrier and peaking PAs in the presence of the HIN. Furthermore, a step-by-step design guide to designing a harmonic injection DPA (HI-DPA) is also presented. It is noted that the passive load provided by the output matching network (Z'_{c2} and Z'_{p2}), the electrical length of the HIN (θ_{inj}), and the phase difference between the currents of the carrier and peaking PAs (θ_p) at the second harmonic are crucial to present an active load to either the carrier or peaking PAs. In the HI-DPA, it is not possible to achieve an active second harmonic load for the carrier and peaking PAs simultaneously. Due to the interaction between the carrier and peaking PAs at the second harmonic, if the carrier PA sees an active load, the peaking PA sees a passive load, and vice-versa. The HI-DPA is designed with the HIN, and its performance is compared with the high-efficiency passive harmonic-tuned DPA. It is demonstrated that both the carrier and peaking PAs cannot see an active impedance at the second harmonic simultaneously. However, it is possible to increase the efficiency in the Doherty load-modulation region with the harmonic injection technique using the HIN. This would be translated into an average efficiency increase when the PA is excited with the modulated signal.

INDEX TERMS Doherty power amplifier, active harmonic injection, high efficiency, continuous class F.

I. INTRODUCTION

In wireless base stations, the RF power amplifier (PA) dominates the overall power consumption. Therefore, there is a great need to improve the efficiency of a PA. Harmonic tuning is a popular technique to achieve high efficiency [1], [2]. In high-efficiency PA modes such as class F, class F^{-1}, and class E, the harmonic tuning is used to engineer the voltage and current waveforms to reduce power dissipation [3], [4], [5]. Harmonic tuning can also be achieved with active harmonic injection [6], [7], [8], [9], [10], [11].

In harmonic injection power amplifiers (HI-PA), the second harmonic ($2f_0$) component is injected at the drain of the transistor to engineer the voltage/current waveforms similar to harmonic tuning. In [6], [7], [8], and [9], the $2f_0$ current is generated from an additional PA operating at $2f_0$ frequency, which is then injected at the drain of the transistor in the main PA. In [10] and [11], an active frequency doubler is used to generate the $2f_0$ current. In all the works previously mentioned, an additional transistor is used, which consumes power and reduces the overall increment in the efficiency of the complete arrangement. Furthermore, the experimental results of these HI-PAs have only been able to enhance their efficiency when operating at full-power, which makes them unsuitable for modern wireless communication systems.

The Doherty power amplifier (DPA) uses two transistors to perform load modulation at the fundamental (f_0) frequency,

The associate editor coordinating the review of this manuscript and approving it for publication was Rocco Giofrè.

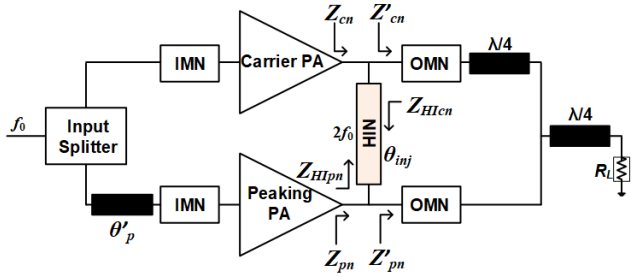

FIGURE 1. Harmonic Injection Doherty Power Amplifier (HI-DPA) configuration.

keeping a high efficiency from a certain output power back-off (OBO) level up to full-power [12], [13]. The two transistors that are already present in the DPA can be used to perform the active harmonic injection, i.e., the harmonic component generated by one transistor can be injected into the drain of the other.

The active harmonic injection Doherty power amplifier (HI-DPA) was proposed in [14], where the $2f_0$ current of one PA is injected into the drain of the transistor of the other PA through a harmonic injection network (HIN). The configuration of the HI-DPA is shown in Fig. 1. The HI-DPA reported in [14] has increased the efficiency in the Doherty region and extended the back-off range. Modified HIN topologies were presented in [15] and [16] to enhance the bandwidth of [14]. In [17], the $2f_0$ current generated by an external PA is injected at the drain of the transistor of the peaking PA, which has increased the small-signal gain and efficiency of the HI-DPA.

Unfortunately, the comparison between the HI-DPA with active harmonic injection and conventional DPA with passive second harmonic termination is not fair in [14], [15], [16], and [17]. The power consumption of the external PA is not considered in the efficiency calculation in [17]. In addition, the conventional DPAs used as a reference in the studies of [14], [15], [16], and [17] to show the improvement in the performance due to their proposed HI-DPA topology have low efficiencies of 55-60% at full-power and 40-45% at back-off. This implies that the $2f_0$ loads selected in the reference case are not optimum for efficiency and therefore the comparison is not fair.

DPAs designed with passive harmonic terminations, such as class F and class F^{-1} [18], have achieved higher efficiencies than the reference DPAs used in these studies. Moreover, the passive $2f_0$ termination of the output matching networks (OMNs) (Z'_{c2} and Z'_{p2} in Fig. 1), which are crucial to determining the loads seen at the drain (Z_{c2} and Z_{p2} in Fig. 1) are not specified in the previous studies. It is possible that the performance enhancement from the reference case achieved with the HIN in these previous works is due to the optimum passive $2f_0$ loads, which can also be achieved with passive harmonic tuning. Unlike passive harmonic tuning, the HIN presents $2f_0$ loads that vary with the input power. But, it is not clear if the performance enhancement with HIN is due to passive $2f_0$ loads, active $2f_0$ loads, or variation of $2f_0$ loads with the input power. The previous studies lack to explain the mechanism of the DPA with HIN and, therefore, do not allow us to verify the true value of the HI-DPA. Therefore, a theoretical analysis and a fair comparison are needed to determine if HI-DPA outperforms conventional DPA with optimum passive harmonic terminations.

This paper aims to overcome these shortcomings of previous works. The main contribution of this paper compared to other HI-DPAs is the comprehensive analysis of the HI-DPA and analysis of the true performance improvement of HI-DPA compared to highly efficient conventional DPA. For that, first, a mathematical relation is established between the passive load provided by the OMN (Z'_{c2} and Z'_{p2}), the electrical length of the HIN (θ_{inj}), and the phase difference between the currents of the carrier and peaking PAs (θ_p), which determines the $2f_0$ load seen by the drain of the carrier (Z_{c2}) and peaking (Z_{p2}) PAs. Using this relationship, it is noted that the $2f_0$ load seen by the carrier and peaking PAs cannot be active simultaneously.

To analyze the HI-DPA's performance, a simplified transistor model consisting of a voltage-dependent current source and a non-linear output capacitance is used. Using this simplified model, a HI-DPA is designed, and its performance is compared with a passive harmonic tuned DPA (HT DPA) designed with continuous class F (CCF) loads for the carrier and peaking PAs. When the carrier PA sees an active $2f_0$ load, its output power and efficiency increase compared to a CCF carrier PA. However, due to the interaction with the carrier PA, the peaking PA sees a passive $2f_0$ load, thereby decreasing output power and efficiency from the CCF case. By carefully choosing the Z'_{c2}, Z'_{p2}, θ_{inj}, and θ_p, the overall output power and/or efficiency of HI-DPA can be increased in the Doherty region compared to the passive HT DPA. This work focuses on increasing efficiency while maintaining the output power similar to passive HT DPA and includes a step-by-step design guide to achieving this.

This paper is organized as follows. In Section II, the topology of the HIN and the analysis of the HI-DPA at the second harmonic frequency are presented. Section III investigates the performance of the HI-DPA compared to the passive harmonic tuned DPA and presents the methodology to achieve high efficiency in the Doherty region. Section IV validates the proposed technique with a high-efficiency HI-DPA implementation. Finally, Section V concludes the paper.

II. ANALYSIS AT THE SECOND HARMONIC FREQUENCY

In the HI-DPA, the $2f_0$ component generated by one PA is injected into the other PA through a HIN. This HIN should only operate at $2f_0$ frequency such that the load modulation at f_0 is unaffected. The topology of the HIN used in this study is shown in Fig. 2 (a). Transmission lines TL1, TL2, TL4, and TL5 are quarter-wave transformers at f_0, while TL3 has a characteristic impedance Z_0 and an electrical length of θ_{inj} at $2f_0$. Therefore, the HIN is open-circuited at f_0 (i.e., Z_{HIc1}=Z_{HIp1}=∞), while it injects the $2f_0$ component at

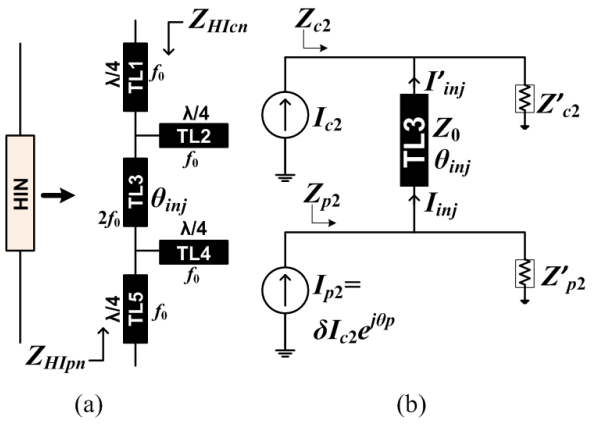

FIGURE 2. (a) Topology of Harmonic Injection Network (HIN). (b) Simplified circuit of the HI-DPA at the second harmonic frequency.

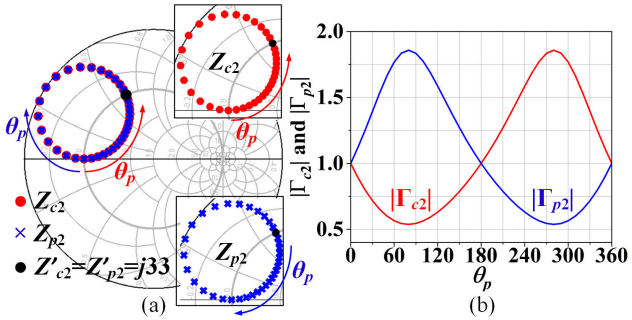

FIGURE 3. Variation of (a) Z_{c2}, and Z_{p2}, and (b) $|\Gamma_{c2}|$ and $|\Gamma_{p2}|$ when θ_p varies from 0° to 360°.

the drain of the other transistor. From Fig. 1 and Fig. 2 (a), the loads seen by the carrier and peaking at f_0 and $2f_0$ can be defined as follows.

$$Z_{cn} = \begin{cases} Z'_{c1}, & @f_0 \\ Z'_{c2}||Z_{HIc2}, & @2f_0 \end{cases} \tag{1}$$

$$Z_{pn} = \begin{cases} Z'_{p1}, & @f_0 \\ Z'_{p2}||Z_{HIp2}, & @2f_0 \end{cases} \tag{2}$$

The simplified circuit of the HI-DPA at $2f_0$ is shown in Fig. 2 (b). The $2f_0$ currents generated by the carrier and peaking PAs are I_{c2} and I_{p2}, respectively. δ and θ_p are the amplitude and phase of the peaking PA with respect to the carrier PA, respectively. The currents in the HIN, before and after TL3, are represented as I_{inj} and I'_{inj}, respectively. The $2f_0$ loads seen by the carrier (Z_{c2}) and peaking (Z_{p2}) PAs can be obtained by solving the HI-DPA circuit shown in Fig. 2 (b) considering the *ABCD* parameters of TL3, as follows,

$$Z_{c2} = \left(1 + \frac{I'_{inj}}{I_{c2}}\right) Z'_{c2} \tag{3}$$

$$Z_{p2} = \left(1 - \frac{I_{inj}}{I_{p2}}\right) Z'_{p2} = \left(1 - \left(\frac{I_{inj}}{I_{c2}} . \frac{1}{\delta e^{j\theta_p}}\right)\right) Z'_{p2} \tag{4}$$

where

$$\frac{I'_{inj}}{I_{c2}} = \frac{\delta e^{j\theta_p} - \frac{Z'_{c2}}{Z'_{p2}} \cos\theta_{inj} - j\frac{Z'_{c2}}{Z_0} \sin\theta_{inj}}{\left(\frac{Z'_{c2}}{Z'_{p2}} + 1\right) \cos\theta_{inj} + j\left(\frac{Z'_{c2}}{Z_0} + \frac{Z_0}{Z'_{p2}}\right) \sin\theta_{inj}} \tag{5}$$

$$\frac{I_{inj}}{I_{c2}} = j\frac{Z'_{c2}}{Z_0} \sin\theta_{inj} + \frac{I'_{inj}}{I_{c2}} \left(\cos\theta_{inj} + j\frac{Z'_{c2}}{Z_0} \sin\theta_{inj}\right) \tag{6}$$

In (3) to (6), Z'_{c2}, and Z'_{p2} are the second harmonic impedances determined by the OMNs of the carrier and peaking PAs, respectively. θ_{inj} is the electrical length of TL3 at $2f_0$. δ is the ratio between the amplitude of the $2f_0$ currents generated by the peaking and the carrier PAs, whose value varies from 0 to 1 when the HI-DPA operates from back-off to full-power in a symmetric DPA configuration. θ_p is the phase difference between the $2f_0$ currents generated by the peaking and the carrier PAs. The phase difference between the input of the peaking and the carrier PAs at f_0 is considered as θ'_p, as shown in Fig. 1. When the carrier and peaking PAs are symmetric, θ_p at $2f_0$ is twice θ'_p at f_0. In the conventional DPA configuration θ'_p is 90° (i.e., $\theta_p = 180°$) [13]. As shown from (3) to (6), the values of Z_{c2}, and Z_{p2} are determined by Z'_{c2}, Z'_{p2}, Z_0, θ_{inj}, δ, and θ_p, which are considered as variables for the analysis.

A. SECOND HARMONIC LOADS WITH θ_P VARIATION

The trajectory of the loads at $2f_0$ Z_{c2}, and Z_{p2} are analyzed by varying θ_p from 0° to 360°. Although this analysis is done at a single frequency, class F load is not suitable for HI-DPA. In class F, $Z'_{c2} = Z'_{p2} = 0$, which will not allow the $2f_0$ current from the peaking PA towards the carrier PA, and vice-versa. Therefore it is assumed that the loads at f_0 and higher harmonics are according to CCF mode; for instance, the passive $2f_0$ loads Z'_{c2} and Z'_{p2} are considered as $j33$ Ω, which corresponds to $\gamma = -0.85$ of the CCF mode [19]. Z_0 and θ_{inj} are taken as 50 Ω and 180°, respectively. δ is considered as 1, which refers to the full-power condition. For the given values, the variation of Γ_{c2} and Γ_{p2} with a variation of θ_p are shown in Fig. 3. $|\Gamma| > 1$ and $|\Gamma| < 1$ imply an active and a passive load, respectively, while $|\Gamma| = 1$ implies a purely reactive load at the edge of the Smith chart. It can be seen from Fig. 3 that Z_{c2} and Z_{p2} are not active simultaneously, i.e., when Z_{c2} is active, Z_{p2} is passive, and vice-versa, as shown in Fig. 3. Z_{c2} and Z_{p2} are at the edge of the Smith chart i.e., $|\Gamma_{c2}| = |\Gamma_{p2}| = 1$, when θ_p is 0°, 180° or 360°. However, $\theta_p = 180°$ is the value for the conventional DPA. Therefore, to present an active load to either carrier or peaking PAs, the value of θ'_p at f_0 should be slightly varied from 90° so that $\theta_p \neq 180°$ at $2f_0$. As the value of θ_p moves away from 0°, 180° or 360°, one PA sees a more active load while the other sees a more passive load, as shown in Fig. 3. However, if θ_p at $2f_0$ is significantly far from 180°, i.e., when θ_p at f_0 is far from 90°, the f_0 currents will be out-of-phase at the output, and the DPA operation will be disturbed. Alternatively, the control of the $2f_0$ with the

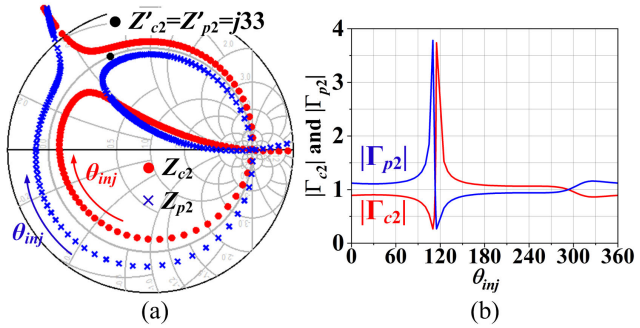

FIGURE 4. Variation of (a) Z_{c2}, and Z_{p2}, and (b) $|\Gamma_{c2}|$ and $|\Gamma_{p2}|$ when θ_{inj} varies from 0° to 360°.

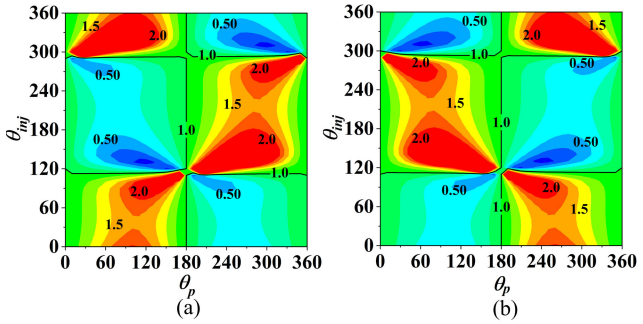

FIGURE 5. Contours of (a) $|\Gamma_{c2}|$ and (b) $|\Gamma_{p2}|$ with different θ_p and θ_{inj}.

nonlinear capacitance at the input may produce θ_p different from 180°, keeping the f_0 currents aligned. However, we have not considered this case to simplify the analysis.

B. SECOND HARMONIC LOADS WITH θ_{INJ} VARIATION

To analyze the variation of Z_{c2} and Z_{p2} with a variation of θ_{inj}; $Z'_{c2} = Z'_{p2} = j33\ \Omega$, $Z_0 = 50\ \Omega$, and $\delta = 1$, are considered. As per the analysis performed in Section II-A, θ_p is taken as 190° to achieve an active $2f_0$ load. The variations of Γ_{c2} and Γ_{p2} with θ_{inj} varying from 0° to 360° are shown in Fig. 4. Again, for any value of θ_{inj}, if Z_{c2} is active, Z_{p2} is passive, and vice-versa. As θ_{inj} increases from 0° to 360°, the Z_{c2} changes from passive to active and then to passive. A similar change can also be seen in Z_{p2} which implies that the direction of the current through the HIN changes twice at the point where $|\Gamma_{c2}| = |\Gamma_{p2}| = 1$, as shown in Fig. 4. It can be noted for this design example that, at $\theta_{inj} \approx 120°$, Z_{c2} and Z_{p2} changes suddenly from highly active to highly passive, and vice-versa. Therefore, for a particular design condition, this region should be identified, and θ_{inj} should be carefully selected.

C. SECOND HARMONIC LOADS WITH θ_P AND θ_{INJ} VARIATION

The active and passive nature of Z_{c2} and Z_{p2} for different values of θ_p and θ_{inj} are verified by considering $Z'_{c2} = Z'_{p2} = j33\ \Omega$, $Z_0 = 50\ \Omega$, and $\delta = 1$. The contours of $|\Gamma_{c2}|$ and $|\Gamma_{p2}|$ with both θ_p and θ_{inj} varying from 0° to 360° are shown in Fig. 5 (a) and (b), respectively. $|\Gamma_{c2}|$ and $|\Gamma_{p2}|$

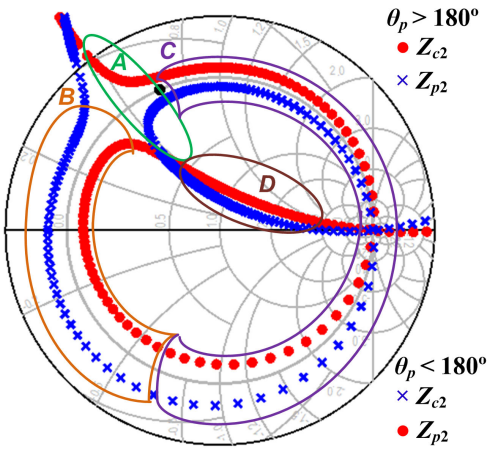

FIGURE 6. Z_{c2} and Z_{p2} in different regions.

that corresponds to 1 is represented by a black line in these contours. The active and passive nature of Z_{c2} and Z_{p2} flips at $\theta_p = 180°$. In other words, for a particular θ_{inj} if Z_{c2} is active for $\theta_p > 180°$, it is passive for $\theta_p < 180°$, as shown in Fig. 5 (a) and (b). As predicted in Section II.A, for any value of θ_{inj}, both Z_{c2} and Z_{p2} are at the edge of the Smith chart (i.e., $|\Gamma_{c2}| = |\Gamma_{p2}| = 1$) when $\theta_p = 180°$. For any value of θ_p and θ_{inj}, the loads seen by the carrier and peaking PAs are either at the edge of the Smith chart (i.e., no harmonic injection) or one PA sees an active while the other sees a passive load. This is also true for other values of Z'_{c2}, Z'_{p2}, Z_0, and δ.

Based on the load trajectories of Z_{c2} and Z_{p2}, the $2f_0$ loads of HI-DPA can be classified into different regions, as shown in Fig. 6. The location of these regions on the Smith chart varies depending on the loads at f_0 and other harmonics. Regions in Fig. 6 are identified, assuming that the loads at f_0 and other harmonics are according to the CCF operation. For $\theta_p > 180°$, Z_{c2} is active and Z_{p2} is passive in region A. Whereas in region B, Z_{c2} is passive while Z_{p2} is active, as shown in Fig. 6. In a CCF PA, the loads corresponding to $|\gamma| > 1$ lead to voltage waveforms with negative peaks and reduce output power and efficiency [19]; this will happen in region C in Fig. 6. In region D, one of the PAs sees a highly passive $2f_0$ load. It is recommended to avoid this region, as output power and efficiency reduce significantly. For $\theta_p < 180°$, the active and passive nature of Z_{c2} and Z_{p2} flips over in all these regions. If loads that correspond to other classes, such as class E or class F^{-1}, are chosen at f_0 and other harmonics, the location of these regions has to change accordingly.

D. SECOND HARMONIC LOADS WITH δ VARIATION

The value of δ is 1 when both carrier and peaking PAs are at full-power. However, at back-off, where the carrier PA is at voltage saturation, and the peaking PA is off, $I_{p2} = 0$, i.e., $\delta = 0$. In the Doherty region, i.e., when the DPA operates from back-off to full-power, δ varies from 0 to 1. The variation of Z_{c2} and Z_{p2} with δ varying from 0 to 1 in regions A, B, and C

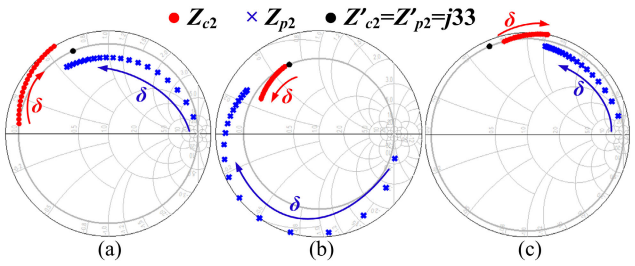

FIGURE 7. Variation of Z_{c2}, and Z_{p2} in (a) region *A* ($\theta_{inj} = 150°$), (b) region *B* ($\theta_{inj} = 50°$), and (c) region *C* ($\theta_{inj} = 250°$), with δ varying from 0 – 1.

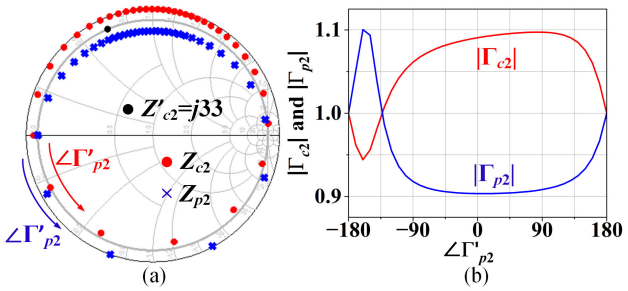

FIGURE 8. Variation of (a) Z_{c2}, and Z_{p2}, and (b) $|\Gamma_{c2}|$ and $|\Gamma_{p2}|$ when $|\Gamma'_{p2}|$ varies from −180° to 180°.

are shown in Fig. 7 (a), (b) and (c), respectively. Here $Z'_{c2} = Z'_{p2} = j33\,\Omega$, $Z_0 = 50\,\Omega$, and $\theta_p = 190°$. In conventional DPA, where HIN is absent, the carrier and peaking PAs only see Z'_{c2} and Z'_{p2}, respectively, at $2f_0$. However, in HI-DPA, even when the peaking is off, i.e., $\delta = 0$, due to the HIN, Z_{c2} sees the parallel combination of Z'_{c2} and Z_{HIc2}, which also depends on Z_0, θ_{inj} and Z'_{p2}. Nevertheless, Z_{c2} is at the edge of the Smith chart for $\delta = 0$, as shown in Fig. 7. As δ increases from 0, Z_{c2} and Z_{p2} become either active or passive. When δ varies from 0 to 1, the trajectory of Z_{c2} and Z_{p2} differs in different regions, as shown in Fig. 7.

E. SECOND HARMONIC LOADS WHEN $Z'_{C2} \neq Z'_{P2}$

In this subsection, the variation of Z_{c2} and Z_{p2} are analyzed when $Z'_{c2} \neq Z'_{p2}$. To perform this analysis, Z'_{c2} is fixed to $j33\ \Omega$, while $\angle\Gamma'_{p2}$ is varied from −180° to 180° to vary Z'_{p2} on the edge of the Smith chart. Here $\theta_p = 190°$, $Z_0 = 50\ \Omega$, $\theta_{inj} = 170°$, and $\delta = 1$ are considered. The corresponding Γ_{c2} and Γ_{p2} are shown in Fig. 8. When $\angle\Gamma'_{p2}$ is ±180°, i.e., when Z'_{p2} is a short-circuit, the peaking PA sees a short-circuit, i.e., $Z_{p2} = 0$. This enforces a short-circuit on the transmission line TL3, and therefore, Z_{c2} sees the parallel combination of Z'_{c2} and short-circuited stub TL3, which is also at the edge of the Smith chart. The direction of current through HIN changes once, other than $\angle\Gamma'_{p2} = \pm 180°$, where both Z_{c2} and Z_{p2} are at the edge of the Smith chart (i.e., $|\Gamma_{c2}| = |\Gamma_{p2}| = 1$), as shown in Fig. 8. It can be seen from Fig. 8 that whenever Z_{c2} is active, Z_{p2} is passive, and vice-versa. For this design example, when $\angle\Gamma'_{p2}$ is selected between −160° to 80°, Z_{c2} and Z_{p2} lie in region *C*, as discussed in Section II-C, which leads to negative peaks in the voltage waveform of the CCF.

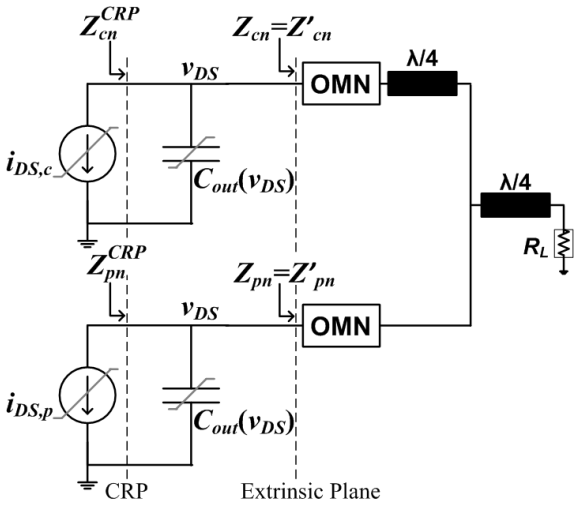

FIGURE 9. Passive HT DPA configuration with simplified transistor model.

Therefore, this comprehensive analysis shows that the combination of design variables Z'_{c2}, Z'_{p2}, Z_0, θ_{inj}, δ, and θ_p should be carefully selected to present a highly active $2f_0$ load to either the carrier PA or the peaking PA, that complies with the selected PA mode.

III. PERFORMANCE ANALYSIS OF HI-DPA

A. PASSIVE HARMONIC TUNING DPA

To compare the performance of the HI-DPA, a high-efficiency conventional DPA is designed with passive harmonic tuning (HT) in the carrier and peaking PAs in the CCF design space [19]. The non-linear output capacitance (C_{out}) influences the performance of CCF PA as presented in [20]. Therefore, a simplified model of a GaN HEMT consisting of a voltage-dependent current source and a non-linear C_{out} is used to verify the theory. Here C_{out} represents all non-linear capacitors at the output of the transistor, i.e., C_{ds} and C_{gd} when the input is short-circuited for all harmonics. The simplified configuration of a passive HT DPA with this model is shown in Fig. 9.

The OMNs of the carrier and peaking PAs are designed to present CCF loads at f_0 and corresponding harmonics at the current-source reference plane (CRP). While calculating the optimum resistance (i.e., $R_{opt} = 2(V_{DD} - V_k)/I_{peak}$), the peak current ($I_{peak}$) is considered as the maximum current (I_{max}) of the device to maximize the output power from the carrier and peaking PAs, for this device $I_{max} \approx 2.1$ A. As discussed in [20], β and γ of the CCF should be carefully mapped in the presence of a nonlinear C_{out}. Therefore $\beta = \alpha/1.92$, and $\gamma = -1$ are chosen at full-power which gives $2f_0$ loads of $Z_{c2}^{CRP} = Z_{p2}^{CRP} = 1.02 + j39.7\ \Omega$ at the CRP [19], [20]. At back-off, R_{opt} is twice that of full-power. If γ at back-off is half of that of full-power, i.e., $\gamma = -0.5$ is considered, the same $2f_0$ loads can be achieved at full-power and back-off, which

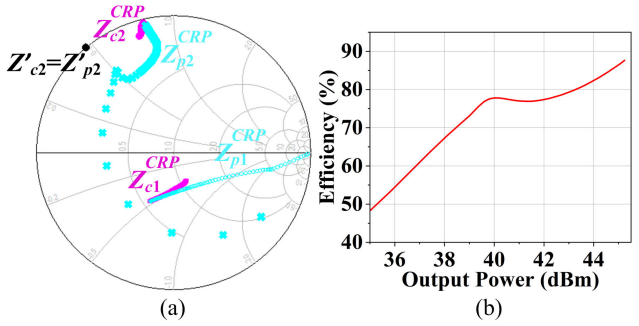

FIGURE 10. (a) Fundamental and second harmonic loads, and (b) Efficiency versus output power of passive HT DPA.

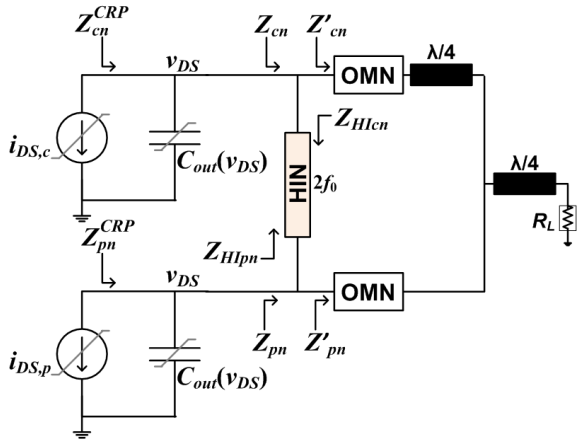

FIGURE 11. DPA with active harmonic injection using HIN.

simplifies the matching at $2f_0$. The selected Z_{c2}^{CRP} and Z_{p2}^{CRP} can be achieved at CRP when $Z'_{c2} = Z'_{p2} = j23.4\ \Omega$ at the extrinsic reference plane (ERP), as shown in Fig. 10 (a). The f_0 and $2f_0$ loads of a passive HT DPA at the CRP are also shown in Fig. 10 (a).

The efficiency versus output power of a passive HT DPA is shown in Fig. 10 (b). With optimum passive $2f_0$ loads, the passive HT DPA has achieved 88% and 75% efficiency at full-power and at 6 dB back-off, respectively, and therefore, allows us to make a fair comparison between passive HT DPA and HI-DPA. In other words, comparison with a passive HT DPA allows us to determine what the HI can do to improve the efficiency of a well-designed DPA and, therefore, its practical significance.

B. ACTIVE HARMONIC INJECTION DPA

The contribution of active harmonic injection on the overall performance of the DPA is analyzed in this sub-section. A HIN is added in between the drain of the transistors in the carrier and peaking PAs, as shown in Fig. 11, which enables the active harmonic injection. At the input of the peaking PA, θ'_p is varied from 90° to achieve $\theta_p \neq 180°$, which enables one of the PAs to see an active $2f_0$ load. θ'_p and θ_{inj} of the HIN are carefully selected, such that one among the

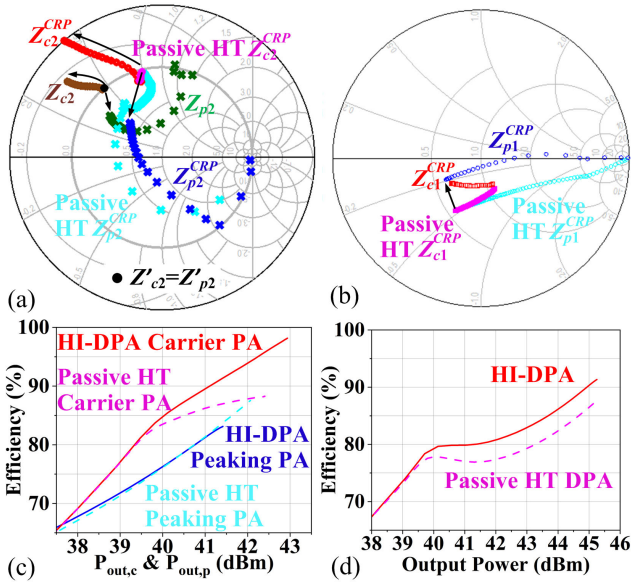

FIGURE 12. (a) Second harmonic loads, (b) Fundamental loads, (c) Efficiency of carrier and peaking PAs, and (d) Overall efficiency of HI-DPA.

carrier and the peaking PAs sees a highly active $2f_0$ load. For the selected design conditions, θ'_p and θ_{inj} are selected as 77° and 51°, respectively, which placed the $2f_0$ loads in region B, as discussed in Section II-C. Due to the HIN, $|\Gamma_{c2}|$ was increased from 1 to 1.35, while $|\Gamma_{p2}|$ was reduced from 1 to 0.74. The $2f_0$ loads for the HI-DPA across power sweep are shown in Fig. 12 (a), the small-signal condition is at the edge of the Smith chart, and progressively evolves into the active and passive region for the carrier and peaking PAs, respectively. Based on the values of θ_p and θ_{inj}, Z_{c2} is active, which also resulted in an active Z_{c2}^{CRP}, as shown in Fig. 12 (a). Z_{c2}^{CRP} now corresponds to $\gamma = -0.5$ and $\beta = \alpha/3.5$ of the CCF mode [19], [20]. Now, based on the new values of γ and β, the f_0 loads of the carrier PA (Z_{c1}^{CRP}) are recalculated, as shown in Fig. 12 (b). In conventional CCF PA, the $2f_0$ load is at the edge of the Smith chart when the design parameter $\beta = \alpha/2$. For $\beta > \alpha/2$, $2f_0$ load is passive, and therefore the output power and efficiency decrease compared to conventional CCF [19]. However, when $\beta < \alpha/2$, $2f_0$ load is active, and the output power and efficiency higher than conventional CCF is achieved [20]. Therefore, due to the active Z_{c2}, the output power and efficiency of the carrier PA are increased as compared to the passive HT DPA, as shown in Fig. 12 (c).

As predicted in Section II, when Z_{c2} is active, Z_{p2} is passive, which also resulted in a passive Z_{p2}^{CRP}, as shown in Fig. 12 (a). Z_{p2}^{CRP} now corresponds to $\gamma = -0.3$ and $\beta = \alpha/1.5$ of the CCF mode. Therefore, based on the new values of γ and β, the f_0 load of the peaking PA (Z_{p1}^{CRP}) need to be recalculated. Since $\beta > \alpha/2$, the output power decreases compared to the passive HT DPA. If $I_{peak} = I_{max}$ is considered for calculating the f_0 load, there will be a negligible change in the dissipated power compared to the

TABLE 1. Comparison between Passive HT DPA and HI-DPA.

Parameter	Passive HT DPA	HI-DPA	
		Carrier PA	Peaking PA
γ	-1	-0.5	-0.3
β	$\alpha/1.92$	$\alpha/3.5$	$\alpha/1.5$
I_{peak}	2.1	2.1	1.8
Z_1^{CRP}	$28.39-j23.76$	$31.97-j11.61$	$29.89-j9.25$
Z_2^{CRP}	$1.02+j39.66$	$-15.38+j21.49$	$18.4+j19.36$
Γ_2^{CRP}	$0.98\angle 103.14°$	$1.69\angle 129.97°$	$0.52\angle 132.69°$
Γ_2	$1\angle 129.84°$	$1.35\angle 141.3°$	$0.74\angle 141.37°$
$P_{out}(W)$	16.75	19.66	13.86
$P_{DC}(W)$	19.05	20.03	16.67
$P_{out,Total}(W)$	$33.5(45.25dBm)$	$33.52(45.253dBm)$	
$P_{DC,Total}(W)$	38.1	36.79	
$P_{diss,Total}(W)$	4.6	3.27	
$\eta(\%)$	88	91.34	

passive HT DPA. Even if there is an improvement in the total output power due to the active $2f_0$ load of the carrier PA, we may not see an increase in the overall efficiency as the dissipated power is almost unchanged. Therefore, to maintain the same total output power as the passive HT DPA while reducing the total dissipated power, I_{peak} is reduced to 1.8 A in the design equations of CCF mode to recalculate the f_0 load of peaking PA, as shown in Fig. 12 (b). Due to $\beta > \alpha/2$ and reduced I_{peak}, the output power and efficiency of the peaking PA reduces compared to the passive HT DPA, as shown in Fig. 12 (c). However, since the overall output power is maintained with a 29% reduction in the total power dissipation, the overall efficiency of the HI-DPA is increased by nearly 3% compared to the passive HT DPA in the entire Doherty region, as shown in Fig. 12 (d). This could be wrongly seen as a small improvement, but since it is in the entire load-modulation zone of the Doherty, an increase of the average efficiency under modulated signal is observed, and a 3% increase in this metric is already significant, especially when the passive design techniques are already saturated. It is worth mentioning that, even though there is a slight phase mismatch between the carrier and peaking PAs due to $\theta_p' \neq 90°$, the HI-DPA has improved the efficiency while still maintaining the overall output power similar to HT DPA. The comparison of the design parameters and the performance of the passive HT DPA and HI-DPA are summarized in Table 1.

When one of the PAs' performance increases due to active $2f_0$ load, the performance decreases in the other PA due to passive $2f_0$ load. Therefore the individual contribution of carrier and peaking PAs on the overall performance of the entire HI-DPA is analyzed in the following two sub-sections.

C. ACTIVE HARMONIC INJECTION IN CARRIER PA

This sub-section studies the contribution of active $2f_0$ load seen by the carrier PA on the overall performance of the DPA. The $2f_0$ current is injected at the drain of the carrier PA using an ideal current source, as shown in Fig. 13. The peaking PA

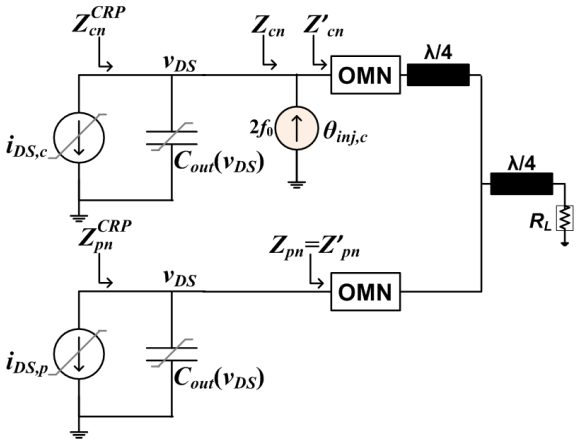

FIGURE 13. DPA with active harmonic injection in carrier PA.

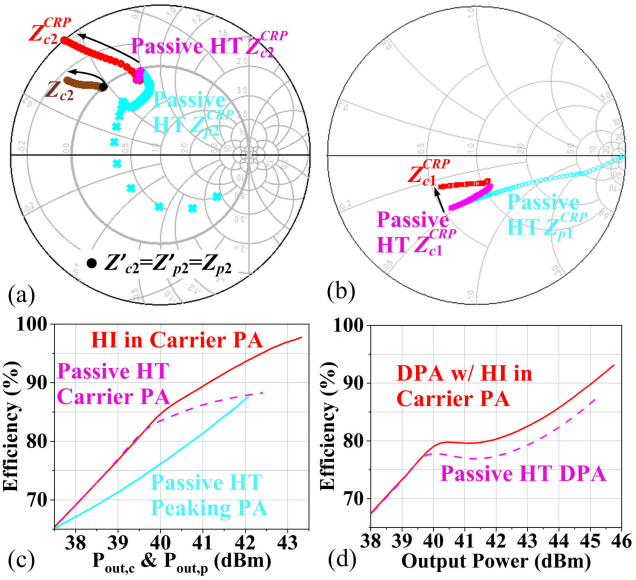

FIGURE 14. (a) Second harmonic loads, (b) Fundamental loads, (c) Efficiency of carrier and peaking PAs, and (d) Overall efficiency of DPA with active harmonic injection in carrier PA.

is assumed to have passive harmonic terminations similar to Section III-A. The phase of the injected $2f_0$ current ($\theta_{inj,c}$) is adjusted such that the value of the active $2f_0$ load at the ERP (Z_{c2}) is the same as the one achieved with the HIN in Section III-B. This resulted in an active Z_{c2}^{CRP} corresponding to $\gamma = -0.5$ and $\beta = \alpha/3.5$ of the CCF mode [19], [20] as shown in Fig. 14 (a). Based on the new values of γ and β, Z_{c1}^{CRP} is recalculated, as shown in Fig. 14 (b), and the OMN of the carrier PA is modified. Due to the active $2f_0$ load, the output power and efficiency of the carrier PA are increased as compared to passive HT DPA, as shown in Fig. 14 (c). Therefore, the overall output power and efficiency of the DPA are increased by 8.7% and 5.2%, respectively, when the carrier PA sees an active $2f_0$ load, as shown in Fig. 14 (d). Note that the power consumption of the $2f_0$ current source is not attributed to the efficiency calculation, as the HIN and the peaking PA will replace the $2f_0$ current source in practice.

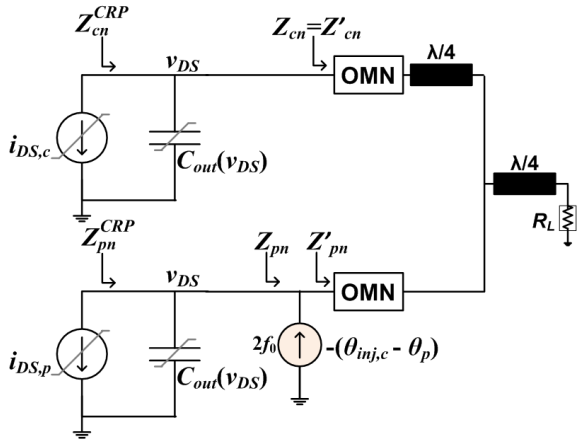

FIGURE 15. DPA with active harmonic injection in peaking PA.

D. ACTIVE HARMONIC INJECTION IN PEAKING PA

When the carrier PA sees an active $2f_0$ load presented in Section III-C, the peaking PA sees a passive $2f_0$ load, according to the analysis in Section II. The impact of this passive $2f_0$ load on the overall performance of the DPA is analyzed by injecting the $2f_0$ current at the drain of the peaking PA, as shown in Fig. 15. The amplitude of the injected $2f_0$ current is the same as that of the carrier PA in Section III-C, but its phase is adjusted such that the value of the passive $2f_0$ load at the ERP (Z_{p2}) is the same as the one achieved with the HIN in Section III-B. The carrier PA is assumed to have passive harmonic loads similar to Section III-A to see the impact of the peaking PA on the overall performance of the DPA. It can be seen from Fig. 16 (a) that the passive Z_{p2}^{CRP} corresponds to $\gamma = -0.3$, $\beta = \alpha/1.5$ and $I_{peak} = 1.8\,A$ of the CCF mode [19], which requires the fundamental load (Z_{p1}^{CRP}) to be recalculated, as shown in Fig. 16 (b). The output power and efficiency of the peaking PA decrease when compared to the passive HT DPA, as shown in Fig. 16 (c). Therefore, degradation can be seen in the overall output power and efficiency of the DPA by 8.6% and 2.3%, respectively, when the peaking PA sees a passive load, as shown in Fig. 16 (d).

Concluding, by carefully choosing the design parameters, the increase and decrease of the output power and efficiency of the two PAs can be wisely balanced so that there is an increase in the overall efficiency of the HI-DPA in the entire Doherty region. The maximum increase in the efficiency of the HI-DPA is approximately 3% even with different combinations of Z'_{c2}, Z'_{p2}, θ_{inj}, and θ_p. It is to be noted that the increase in efficiency is the same even if the peaking PA sees an active load and the carrier PA sees a passive load.

E. DESIGN METHODOLOGY

The methodology to design a HI-DPA is described step-by-step in this sub-section.

The first step is to design a DPA with the best possible passive harmonic terminations similar to the passive HT DPA presented in Section III-A. For example, the passive HT

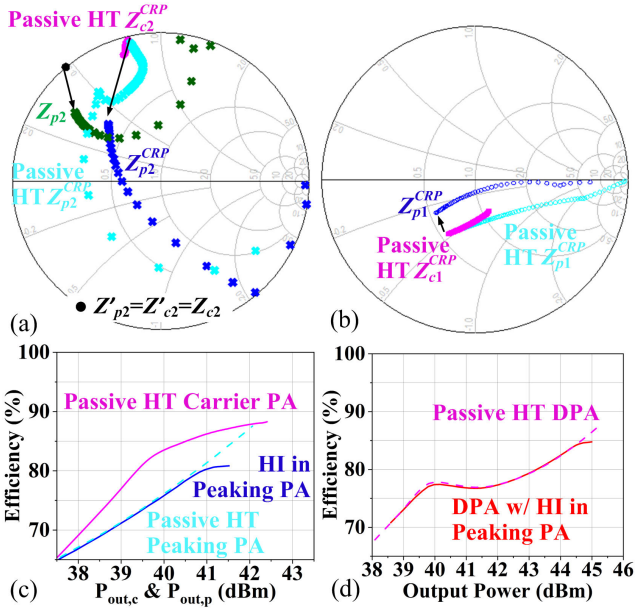

FIGURE 16. (a) Second harmonic loads, (b) Fundamental loads, (c) Efficiency of carrier and peaking PAs, and (d) Overall efficiency of DPA with active harmonic injection in peaking PA.

DPA can be designed with harmonic terminations similar to the CCF.

Step 2 is to design a HIN as described in Section II to present an open-circuit at f_0, but a transparent $2f_0$, with an electrical length of θ_{inj}.

The next step is to add the HIN in between the drain terminals of the carrier and the peaking PAs of the designed passive HT DPA, as shown in Fig. 1.

In step 4, θ'_p, shown in Fig. 1, is adjusted to vary θ_p at $2f_0$ from the conventional DPA value of 180°. When $\theta_p \neq 180°$, at least one among the carrier and the peaking PAs sees an active $2f_0$ load as discussed in Section II. However, θ_p at f_0 should be close to 90° for the f_0 currents of the carrier and peaking PAs to be added in phase at the output of the DPA.

Step 5 is adjusting θ_{inj} to achieve a highly active $2f_0$ load for either the carrier or the peaking PA. For instance, if the carrier and peaking PA see active and passive loads, respectively, then θ_{inj} should be carefully selected such that $|\Gamma_{c2}|$ is as high as possible. In the passive HT DPA designed in step 1, the OMN presents f_0 and harmonic loads corresponding to a particular combination of β and γ. However, due to the HIN, the location of the $2f_0$ loads is changed, which now corresponds to different β and γ, and therefore their combination with the fundamental loads is no longer optimum.

Therefore, in step 6, the f_0 load of the PA that sees an active load should be adjusted based on the change caused by the HIN on the $2f_0$ load. For instance, if the carrier PA sees an active load, Z_{c2}^{CRP} corresponds to different γ and $\beta < \alpha/2$, as compared to the passive HT DPA. Based on these new γ and β, the Z_{c1}^{CRP} is recalculated considering $I_{peak} = I_{max}$ to adjust the OMN of the carrier PA at f_0.

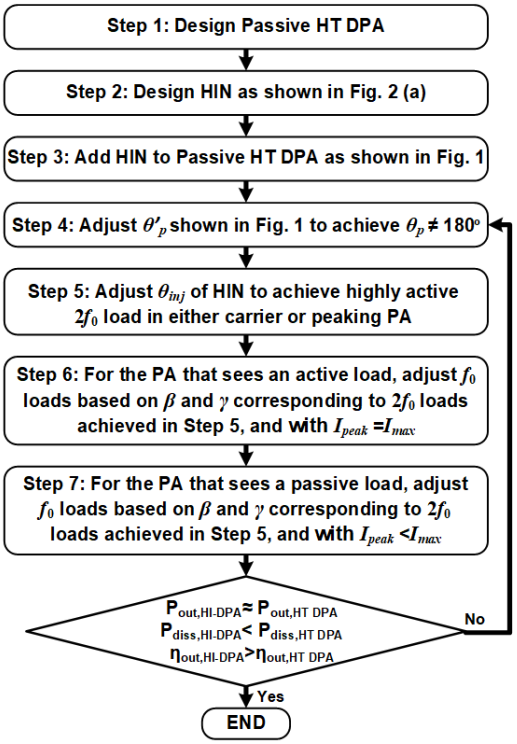

FIGURE 17. Design flow of HI-DPA.

Now, in step 7, the f_0 load is adjusted for the PA that sees a passive $2f_0$ load due to the HIN. If the peaking PA sees a passive load, Z_{p2}^{CRP} corresponds to different γ and $\beta > \alpha/2$. Z_{p1}^{CRP} is recalculated for new γ and β; however, with $I_{peak} < I_{max}$ to reduce the dissipated power compared to the passive HT DPA. The OMN is adjusted to present this recalculated Z_{p1}^{CRP}.

When the HI-DPA maintains the output power of the passive HT DPA while reducing its power dissipation, it guarantees an increase in efficiency. As a result, the design process can be concluded. If neither the output power is the same as the passive HT DPA nor the efficiency is higher than the passive HT DPA, repeat the process from step 4 until these conditions are met.

Following these design guidelines, one can design a HI-DPA with improved efficiency over an already optimized DPA with passive HT in the Doherty region.

IV. HI-DPA DESIGN AND EXPERIMENTAL VALIDATION

A. DESIGN AND SIMULATION

To illustrate the proposed design methodology, a HI-DPA was designed to operate at 1.5 GHz. The circuit schematic of the designed HI-DPA is shown in Fig. 18. The carrier and peaking PAs use the 10-W GaN HEMT CGH40010F, which has I_{max} of 1.5 A. Both the transistors are biased with 28 V drain voltage. The carrier PA is biased with a gate voltage of -3.1 V to draw a quiescent drain current of 34.5 mA, and the gate bias of the peaking PA is set to -5 V. The OMNs of the carrier and peaking PAs are initially designed to present CCF loads corresponding to $\gamma = 0.5$ and $\gamma = 0.05$, respectively, at 1.5 GHz, at the CRP. The $2f_0$ loads presented by the OMNs at the ERP and CRP are shown in Fig. 19 (a) and (b), respectively. The input matching networks (IMNs) of both PAs are designed to maximize gain without compromising efficiency. The designed carrier and peaking PAs with passive HT are connected in DPA configuration. A Wilkinson power splitter is used to equally divide the RF input power to the carrier and peaking PAs, as shown in Fig. 18.

Transmission line TL1 used at the IMN of the peaking PA has a phase of $\theta'_p = 78°$ which makes $\theta_p \neq 180°$ and achieves an active $2f_0$ load, as per the proposed design methodology. The HIN is designed and added to the HI-DPA, as shown in Fig. 18. Transmission lines TL2 to TL5 are designed as quarter-wave transformers at 1.5 GHz, which makes the carrier and peaking PAs see an open-circuit through the HIN at 1.5 GHz. The phase of the transmission line TL6 is selected as $\theta_{inj} = 86°$ at 3 GHz, which presents an active $2f_0$ load to the peaking PA at the ERP and the CRP, as shown in Fig. 19 (a) and (b), respectively. Due to the HIN, the $2f_0$ load of the peaking PA now corresponds to $\gamma = 0.45$, and $\beta = \alpha/2.25$ of the CCF mode [19]. Therefore, the fundamental load of the peaking PA is redesigned based on the new values of γ and β with $I_{peak} = I_{max} = 1.5\ A$, as shown in Fig. 19 (c). According to the presented theory, the main PA now sees a passive $2f_0$ load, as shown in Fig. 19 (a) and (b). The main PA now sees $2f_0$ load corresponding to $\gamma = 0.9$ and $\beta = \alpha/1.77$. Therefore, the fundamental load of the carrier PA is redesigned based on the new values of γ and β, but with $I_{peak} = 1.2\ A$ to reduce the total dissipated power, as discussed in Section III-E.

The comparison between the simulated results of the passive HT DPA and the HI-DPA is shown in Fig. 19 (d). The HI-DPA achieved a drain efficiency (DE) of 80%, corresponding to the output power of 43 dBm. At 6 dB output power back-off (OBO), the DE is 62.5%. The gain at saturation is 10.5 dB. It can be seen from Fig. 19 (d) that the DE of HI-DPA is improved compared to the passive HT DPA by 3.5% in the Doherty region. The simulated voltage and current waveforms of the carrier and peaking PAs at the CRP at full-power are shown in Fig. 20, which shows the CCF characteristics.

B. EXPERIMENTAL RESULTS

The designed HI-DPA was implemented on a RO4350B substrate with a dielectric constant of 3.66 and thickness of 20 mil. The photograph of the fabricated HI-DPA is shown in Fig. 21 (a). The implemented HI-DPA was measured with pulsed continuous wave (CW) and modulated signals for experimental validation. The measured DE and gain over the obtained output power are shown in Fig. 21 (b). The measured DE is 78% at the saturated output power of 43 dBm, while at 6 dB OBO, the DE is 60%. The measured gain at saturation is 7 dB, as shown in Fig. 21 (b).

The HI-DPA is also tested with a 3 MHz long-term evolution (LTE) signal with a peak-to-average power ratio

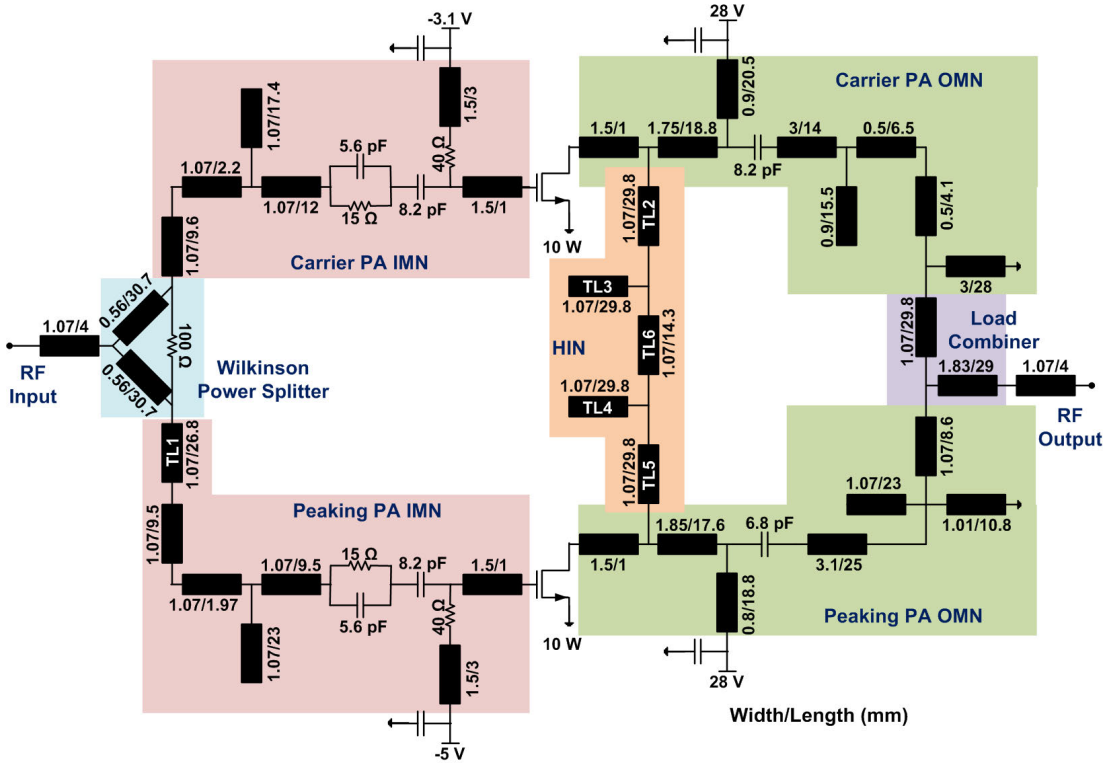

FIGURE 18. Circuit schematic of designed HI-DPA.

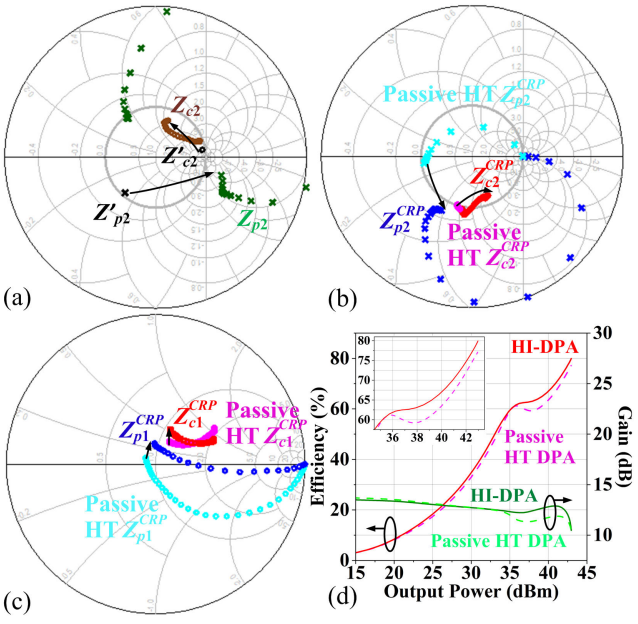

FIGURE 19. (a) Second harmonic loads at the ERP, (b) Second harmonic loads at CRP, (c) Fundamental loads at CRP, and (d) Simulated efficiency and gain of passive HT DPA and HI-DPA.

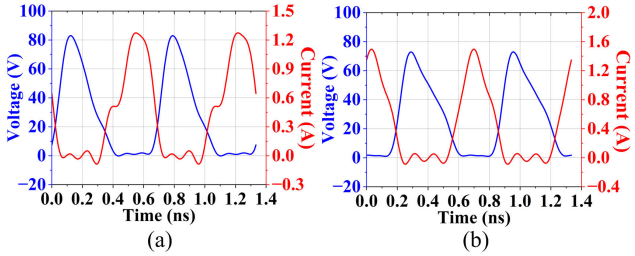

FIGURE 20. Voltage and current waveforms of (a) Carrier PA and (b) Peaking PA of HI-DPA at full-power.

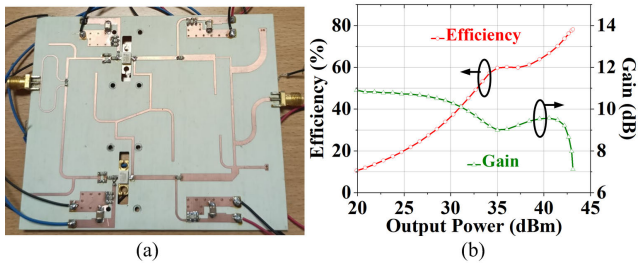

FIGURE 21. (a) Photograph of implemented HI-DPA, and (b) Measured efficiency and gain of implemented HI-DPA.

(PAPR) of 8.5 dB. The measured output power spectral density at 1.5 GHz without and with DPD is shown in Fig. 22. The HI-DPA achieves an average output power of 34.9 dBm and an average efficiency of 55.3% with DPD. The measured adjacent channel power ratio (ACPR) is −30 dB without DPD, which is improved to −59 dB with DPD.

Table 2 shows the comparison of the implemented PA with other HI-DPAs. As shown in Table 2, the performance of this work is comparable to the state-of-art HI-DPAs.

TABLE 2. Comparison with State-of-the-art harmonic injection doherty power amplifiers.

Ref.	Freq. (GHz)	P_{out} @ FP (dBm)	OBO (dB)	Eff @ FP (%)	Eff @ BO (%)	ACPR without DPD (dB)	ACPR with DPD (dB)
[14]	1.6-1.9	42-43	10-10.6	78.3-83	46-46.3	-32	-53.3
[15]	1.4-2.1	42.8-43.5	6	65-85	60-65	-42 to -28	-
[16]	1.6-1.95	42.7-43.5	9	64.6-70.9	62.5-67.5	-22	-
This work	1.5	43	6	78	60	-30	-59

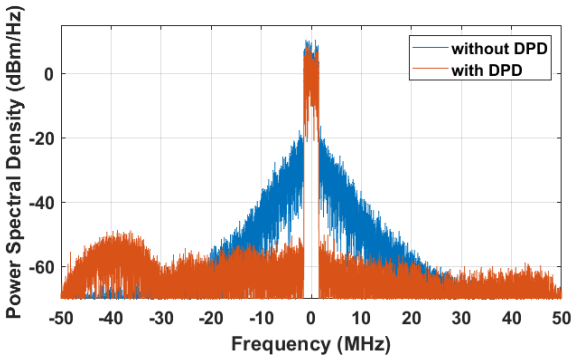

FIGURE 22. Output spectrum from modulated measurement using 3 MHz 8.5 dB PAPR LTE signal for 1.5 GHz.

Nevertheless, the main contribution of this work is to present a comprehensive analysis of HI-DPA compared to the high-efficiency passive HT DPA and a step-by-step design methodology to design a HI-DPA, which are not found in other works. The interesting future scope of this work is to extend it for wider bandwidth by modifying the topology of the HIN, and by designing wideband matching networks and wideband Doherty combiner.

V. CONCLUSION

This paper has shown that the mutual injection of second harmonic current between the carrier and peaking PAs of the Doherty power amplifier will present the $2f_0$ load either at the edge of the Smith chart or an active load to one PA and a passive load to the other. It is understood from the second harmonic analysis of the HI-DPA that the $2f_0$ loads seen by the carrier and peaking PAs depend on the passive load provided by the output matching networks (Z'_{c2} and Z'_{p2}), the electrical length of the HIN (θ_{inj}), and the phase difference between the $2f_0$ currents of the carrier and peaking PAs (θ_p). By a wise choice of design variables, the decrease in the performance due to the passive $2f_0$ load of one PA can be balanced out with the active $2f_0$ load of the other PA to improve the efficiency in the Doherty region without compromising the output power.

REFERENCES

[1] P. Colantonio, F. Giannini, and E. Limiti, *High Efficiency RF and Microwave Solid State Power Amplifiers*. Hoboken, NJ, USA: Wiley, 2009.

[2] P. Wright, J. Lees, J. Benedikt, P. J. Tasker, and S. C. Cripps, "A methodology for realizing high efficiency class-J in a linear and broadband PA," *IEEE Trans. Microw. Theory Techn.*, vol. 57, no. 12, pp. 3196–3204, Dec. 2009.

[3] F. H. Raab, "Class-F power amplifiers with maximally flat waveforms," *IEEE Trans. Microw. Theory Techn.*, vol. 45, no. 11, pp. 2007–2012, Feb. 1997.

[4] F. H. Raab, "Maximum efficiency and output of class-F power amplifiers," *IEEE Trans. Microw. Theory Techn.*, vol. 49, no. 6, pp. 1162–1166, Jun. 2001.

[5] F. Raab, "Idealized operation of the class E tuned power amplifier," *IEEE Trans. Circuits Syst.*, vol. CS-24, no. 12, pp. 725–735, Dec. 1977.

[6] A. AlMuhaisen, P. Wright, J. Lees, P. J. Tasker, S. C. Cripps, and J. Benedikt, "Novel wide band high-efficiency active harmonic injection power amplifier concept," in *IEEE MTT-S Int. Microw. Symp. Dig.*, May 2010, pp. 664–667.

[7] A. AlMuhaisen, J. Lees, S. C. Cripps, P. J. Tasker, and J. Benedikt, "Wide band high-efficiency power amplifier design," in *Proc. 6th Eur. Microw. Integr. Circuit Conf.*, Oct. 2011, pp. 184–187.

[8] A. Dani, M. Roberg, and Z. Popovic, "PA efficiency and linearity enhancement using external harmonic injection," *IEEE Trans. Microw. Theory Techn.*, vol. 60, no. 12, pp. 4097–4106, Dec. 2012.

[9] M. Seo, H. Lee, J. Gu, H. Kim, J. Ham, W. Choi, Y. Yun, and Y. Yang, "High-efficiency power amplifier using an active second-harmonic injection technique under optimized third-harmonic termination," *IEEE Trans. Circuits Syst. II, Exp. Briefs*, vol. 61, no. 8, pp. 549–553, Aug. 2014.

[10] Y. M. A. Latha, K. Rawat, M. Helaoui, and F. M. Ghannouchi, "Broadband continuous mode power amplifier with on-board harmonic injection," *IET Microw., Antennas Propag.*, vol. 13, no. 9, pp. 1402–1407, Jul. 2019.

[11] Y. M. Asha Latha and K. Rawat, "Methodology to realize wideband high efficiency power amplifier using active harmonic injection," in *IEEE MTT-S Int. Microw. Symp. Dig.*, Dec. 2019, pp. 1–4.

[12] W. H. Doherty, "A new high-efficiency power amplifier for modulated waves," *Bell Syst. Tech. J.*, vol. 15, no. 3, pp. 469–475, Jul. 1936.

[13] B. Kim, *Doherty Power Amplifiers: From Fundamentals to Advanced Design Methods*. New York, NY, USA: Academic, 2018.

[14] X. Y. Zhou, S. Y. Zheng, W. S. Chan, X. Fang, and D. Ho, "Postmatching Doherty power amplifier with extended back-off range based on self-generated harmonic injection," *IEEE Trans. Microw. Theory Techn.*, vol. 66, no. 4, pp. 1951–1963, Apr. 2018.

[15] X. Y. Zhou, W. S. Chan, S. Y. Zheng, W. Feng, H.-Y. Liu, K. M. Cheng, and D. Ho, "A mixed topology for broadband high-efficiency Doherty power amplifier," *IEEE Trans. Microw. Theory Techn.*, vol. 67, no. 3, pp. 1050–1064, Mar. 2019.

[16] X. Zhou, W. S. Chan, T. Sharma, J. Xia, S. Chen, and W. Feng, "A Doherty power amplifier with extended high-efficiency range using three-port harmonic injection network," *IEEE Trans. Circuits Syst. I, Reg. Papers*, vol. 69, no. 7, pp. 2756–2766, Jul. 2022.

[17] M. S. Mugisho, S. K. Maity, C. Friesicke, and R. Quay, "Harmonic-injection Doherty power amplifiers with a high small-signal gain," in *Proc. Int. Workshop Integr. Nonlinear Microw. Millimetre-Wave Circuits (INMMiC)*, Apr. 2022, pp. 1–3.

[18] J. Kim, "Highly efficient asymmetric class-F^{-1}/F GaN Doherty amplifier," *IEEE Trans. Microw. Theory Techn.*, vol. 66, no. 9, pp. 4070–4077, Sep. 2018.

[19] V. Carrubba, A. L. Clarke, M. Akmal, J. Lees, J. Benedikt, P. J. Tasker, and S. C. Cripps, "On the extension of the continuous class-F mode power amplifier," *IEEE Trans. Microw. Theory Techn.*, vol. 59, no. 5, pp. 1294–1303, May 2011.

[20] Y. M. Asha Latha, L. C. Nunes, F. M. Barradas, and J. C. Pedro, "The role of nonlinear cout in continuous class F PAs," in *IEEE MTT-S Int. Microw. Symp. Dig.*, Jun. 2023, pp. 579–582.

Y. MARY ASHA LATHA (Member, IEEE) was born in India, in 1991. She received the M.Tech. degree (Hons.) in electronics and communication engineering from the National Institute of Technology Hamirpur (NIT), Hamirpur, India, in 2015, and the Ph.D. degree from Indian Institute of Technology (IIT) Roorkee, India, in 2021. From November 2021 to March 2023, she was a Postdoctoral Researcher with the Institute of Telecommunications, Aveiro, Portugal. Her current research interests include the design of high-efficiency and wideband RF power amplifiers with harmonic manipulation and GaN MMIC circuits. Her research has resulted in one patent and 15 publications in international journals and conferences. She was a recipient of various awards, including the 2019 MTT-S IMaRC Student Best Paper Award and the 2023 MTT-S IMS Early Career Paper Competition Finalist. She has been a reviewer of several IEEE and IET journals, and conferences.

LUÍS C. NUNES (Senior Member, IEEE) was born in Portugal, in 1986. He received the M.Sc. and Ph.D. degrees in electrical engineering from Universidade de Aveiro, Aveiro, Portugal, in 2010 and 2015, respectively. From 2016 to 2017, he was an RF Design Engineer with Huawei Technologies, Sweden. He is currently a Researcher Assistant with the Institute of Telecommunications, Universidade de Aveiro. His main research interests include active device modeling, nonlinear distortion analysis, and the design of microwave circuits, especially high-efficiency and linear power amplifiers. He was a recipient of the 2022 EuMIC Best Paper Award and the 2024 Microwave Prize. He has served as a reviewer for several IEEE journals and conferences.

FILIPE M. BARRADAS (Member, IEEE) was born in Évora, Portugal, in July 1989. He received the M.Sc. degree in electronics and telecommunications engineering and the Ph.D. degree in electrical engineering from Universidade de Aveiro, Aveiro, Portugal, in 2012 and 2017, respectively. He is currently a Research Assistant with the Instituto de Telecomunicações, Universidade de Aveiro. His main research interests include digital predistortion and behavioral modeling of radio frequency power amplifiers (RF PAs), and signal processing with applications on telecommunications. His other interests include the design and analysis of nonlinear microwave circuits. He has been a reviewer of several IEEE journals.

JOSÉ C. PEDRO (Fellow, IEEE) received the Diploma, Ph.D., and Habilitation degrees in electronics and telecommunications engineering from Universidade de Aveiro, Aveiro, Portugal, in 1985, 1993, and 2002, respectively. He is currently a Full Professor with Universidade de Aveiro and the President of the Instituto de Telecomunicações, Universidade de Aveiro. He has authored two books and authored or coauthored more than 200 articles in international journals and symposia. His current research interests include active device modeling and the analysis and design of various nonlinear microwave circuits. He was a recipient of various prizes, including the 1993 Marconi Young Scientist Award, the 2000 Institution of Electrical Engineers Measurement Prize, the 2015 EuMC Best Paper Microwave Prize, and the Microwave Distinguished Educator Award. He has served the scientific community as a Reviewer and an Editor for several conferences and journals, namely, IEEE Transactions on Microwave Theory and Techniques, for which he was the Editor-in-Chief.